

Optimal Control of Vibration-Based Micro-energy Harvesters

Thuy T. T. Le¹ · Felix Jost¹ · Sebastian Sager¹

Received: 20 August 2017 / Accepted: 13 February 2018 / Published online: 12 March 2018
© Springer Science+Business Media, LLC, part of Springer Nature 2018

Abstract We analyze the maximal output power that can be obtained from a vibration energy harvester. While recent work focused on the use of mechanical nonlinearities and on determining the optimal resistive load at steady-state operation of the transducers to increase extractable power, we propose an optimal control approach. We consider the open-circuit stiffness and the electrical time constant as control functions of linear two-port harvesters. We provide an analysis of optimal controls by means of *Pontryagin's maximum principle*. By making use of geometric methods from optimal control theory, we are able to prove the *bang–bang* property of optimal controls. Numerical results illustrate our theoretical analysis and show potential for more than 200% improvement of harvested power compared to that of fixed controls.

Keywords Optimal control · Pontryagin's maximum principle · Switching function · Energy harvesting · Power optimization

Mathematics Subject Classification 49K15 · 49J30 · 93B40

Communicated by Lars Grüne.

✉ Sebastian Sager
sager@ovgu.de

Thuy T. T. Le
thuy.lethien@ovgu.de

Felix Jost
felix.jost@ovgu.de

¹ Institute of Mathematical Optimization, Mathematical Algorithmic Optimization, Otto-von-Guericke University, 39106 Magdeburg, Germany

1 Introduction

Most of the energy used in electronics and sensor applications is supplied by batteries, which are very limited in operational lifetime. Additionally, there are several environments where battery performance is especially limiting. Energy harvesting therefore becomes a key alternative for replacing battery roles in autonomous sensor networks [1,2]. Due to the capability of providing electrical power harvested from mechanical vibration sources for electronic devices, energy harvesters are more and more central to recent research. Energy storage cells such as rechargeable batteries or super-capacitors cannot intrinsically ensure optimal power generation if directly connected to rectifier output. A solution for the power optimization problem was proposed by Ottman et al. [3], using a dc-dc converter interleaved between the rectifier and the storage cells. They have shown that the optimal power point can be tracked by controlling the converter input average resistance. The power of a vibration-based generator strongly depends on the load. The power is maximized by matching load resistances, whose values are determined by the transducer figure of merit, external acceleration and vibration frequency [4]. A detailed discussion of optimizing power generated by a velocity damped resonant generator (VDRG), taking into account both of mechanical damping and electrical damping, is reported by Mitcheson et al. [5]. In summary, for unconstrained displacement or small forcing levels, and significant mechanical damping, the harvested power can be maximized by designing the electrical damping equal to the mechanical damping while the drive frequency is kept fixed at resonant frequency. A bound on the output power of vibration energy harvesters when the proof mass is subject to parasitic, linear mechanical damping is determined in closed form [6]. Halvorsen et al. proved that the optimal VDRG performance for a single sinusoid forcing coincides with the bound when the displacement is unconstrained. The same methodology is used to find the upper bound as a function of input vibration parameters with two more additional study cases, double sinusoid input and frequency-swept sinusoid input [7]. An analytical expression of the optimal load and stiffness of a linear two-port harvester driven by harmonic force under displacement-constrained operation was obtained in [8]. With the same perspectives, the optimal gap and load of the micro-electricity generator are also proved to be dependent on the proof mass displacement amplitude versus its limit [9].

Several efforts to optimize the scavenged power can be listed, such as analytical solutions and experimental validations of distributed-parameter optimization in piezoelectric energy harvesting by Erturk et al. [10]. An advanced device concept for micro-scale electrostatic energy harvester utilizing active end-stops as secondary transducers is reported by Le et al. [11]. von Büren and Tröster [12] developed a two-stage optimization method which allows optimization of geometry, resonance frequency and electrical load for a linear electromagnetic micro-power generator architecture.

However, research work mentioned above only examines the energy balance of the harvesting systems in steady state, which allows us to neglect the kinetic energy of the proof mass and the potential energy stored in the transducers. If the external driving force contains an amplitude that is varying over time, the complex conjugate matching method no longer works. Such situations will be investigated in this paper. From the mathematical point of view, the linear two-port model consists of a strongly

stiff system of ordinary differential equations (ODEs) due to the high frequency of the displacement. This causes difficulties in solving the problem numerically. Therefore, obtaining the approximate optimal power is a demanding task. The question of which values the stiffness and the electrical time constant should take in order to obtain maximized output power is studied analytically by classical methods in control theory, namely Pontryagin’s maximum principle and geometric methods of optimal control theory, see for instance [13,14]. Some applications of these methods for investigating optimization problems in medicine can be mentioned, such as antiangiogenic therapy in cancer treatment [15], the optimal delivery of combination therapy for tumors [16], a multi-input optimal control problem for combinations of cancer chemotherapy with immunotherapy in form of a boost to the immune system [17], or in optimal experimental design problems [18]. Their applications in economics can be found in [19,20].

The structure of this paper is as follows. First, the linear two-port model is introduced. Then the analysis of optimal controls for this model is presented. We finally end up with solving the power optimization problems numerically under different settings with and without constraints, together with a discussion to show how the numerical results confirm our theoretical analysis and how much the output power can be improved by our approach.

2 Mathematical Model

An example of a real electromechanical system is an overlap varying capacitance structure. The basic configuration of such an electrostatic energy harvester is shown in Fig. 1. The design consists of a proof mass suspended by four linear springs. The transducers are operated by an external bias voltage connected to the movable mass. The output power is harvested by conversion from mechanical to electrical energy using capacitive transduction. The fixed electrodes are connected directly to external loads. Due to practical restrictions on device dimensions, mechanical end-stops are used to limit the proof mass motion and avoid beam fracture.

Fig. 1 An electrostatic in-plane overlap varying energy harvester, an example of an electromechanical transducer

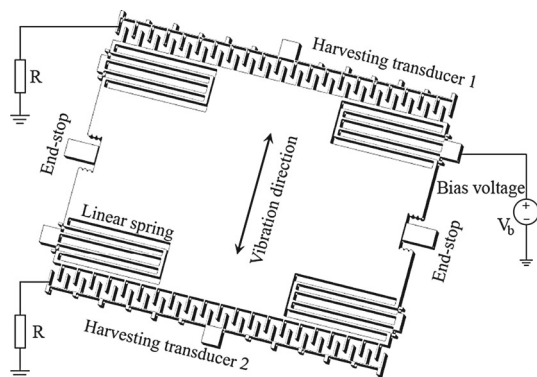
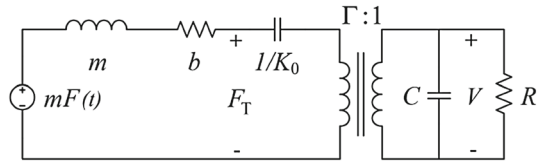


Fig. 2 Electrical equivalent circuit of the linear two-port model



Transducers with three common mechanisms, i.e., piezoelectric, electrostatic and electromagnetic conversions, can be described by the linear two-port model with a single degree of freedom. The harvester is now no longer represented by complex differential equations and boundary conditions, but by a lumped-element circuit [21]. The elements are representatives of the transducer properties such as mass, stiffness, parasitic damping and variable capacitance. Equivalent circuits are widely used nowadays along with powerful mathematical techniques and network analysis programs, for instance LT-SPICE (Simulation Program with Integrated Circuit Emphasis) which is used to generate a reference solution in Sect. 4. Typically, an electrostatic energy generator can be modeled as a kinetic harvester with a generic transducer force F_T acting on the proof mass. The linear two-port equations for such a harvesting system are expressed as in [8]

$$F_T(t) = Kx(t) + \frac{\Gamma}{C}q(t), \quad V(t) = \frac{\Gamma}{C}x(t) + \frac{1}{C}q(t) \tag{1}$$

where K is the open-circuit stiffness, $x(t)$ is the displacement, $q(t)$ is the charge on the electrode, C represents the variable capacitor, Γ is the transduction factor and $V(t)$ is the voltage across the electrical port. Figure 2 depicts the equivalent circuit of the electrostatic generator, whereas the inertial mass m is subject to external forcing function $F(t)$ and the parasitic damping b . A load resistance R is connected directly to the electrical terminal. The short circuit stiffness K_0 is related to the open-circuit stiffness K by $K_0 = (1 - k^2)K$, where the coupling factor is given by $k^2 = \frac{\Gamma^2}{KC}$.

Considering the open-circuit stiffness and the load resistance as *time-dependent functions*, the power optimization problem on a fixed time horizon $[t_0, t_f]$ is formulated as follows

$$\max_{x(t), V(t), R(t), K(t)} \left(\frac{1}{t_f - t_0} \int_{t_0}^{t_f} \frac{V(t)^2}{R(t)} dt \right)$$

subject to

$$m\ddot{x}(t) = - \left(K(t) - \frac{\Gamma^2}{C} \right) x(t) - b\dot{x}(t) - V(t)\Gamma + mF(t), \tag{2}$$

$$\dot{V}(t) = \frac{\Gamma}{C}\dot{x}(t) - \frac{1}{R(t)C}V(t),$$

$$K(t) \in [\underline{K}, \overline{K}], \quad R(t) \in [\underline{R}, \overline{R}],$$

$$(x(t_0), V(t_0)) = (x_0, V_0)$$

where $0 \leq t_0 < t_f < +\infty$, $\underline{K} > \frac{\Gamma^2}{C} > 0$, $\underline{R} > 0$, $\overline{K}, \overline{R} < +\infty$ and either

$$F(t) = F_a(t) = A_r t g \cos(\omega t) \quad \text{or} \quad F(t) = F_f(t) = A_c g \cos\left(\omega_0 t + \frac{1}{2} \omega_r t^2\right) \quad (3)$$

with ω is the drive angular frequency, g is the gravitational acceleration, $A_r = \frac{\Delta A}{\Delta t} = \frac{A_f - A_0}{t_f - t_0}$ has units of $g \text{ s}^{-1}$, $\omega_r = \frac{\Delta \omega}{\Delta t} = \frac{\omega_f - \omega_0}{t_f - t_0}$ has units of rad s^{-2} , where A_0 (ω_0) and A_f (ω_f) are acceleration amplitudes (angular frequencies) at t_0 (t_f), respectively. The value of A_c is kept fixed. The preceding problem containing a second-order ordinary differential equation (ODE) can be reduced to the one with merely first-order ODEs equivalently by introducing an auxiliary variable. Moreover, for convenience, let $u_1(t) = K(t)$, $u_2(t) = \frac{1}{R(t)}$. The optimization problem (2) is transformed to the following one.

$$\begin{aligned} & \max_{x(t), y(t), V(t), u_1(t), u_2(t)} \left(\frac{1}{t_f - t_0} P(t_f) \right) \\ & \text{subject to} \\ & \dot{x}(t) = y(t), \\ & \dot{y}(t) = -\frac{1}{m} \left(u_1(t) - \frac{\Gamma^2}{C} \right) x(t) - \frac{b}{m} y(t) - \frac{V(t)\Gamma}{m} + F(t), \\ & \dot{V}(t) = \frac{\Gamma}{C} y(t) - \frac{u_2(t)}{C} V(t), \\ & \dot{P}(t) = V(t)^2 u_2(t), \\ & u_1(t) \in [\underline{u}_1, \overline{u}_1], \quad u_2(t) \in [\underline{u}_2, \overline{u}_2] \\ & (x(t_0), y(t_0), V(t_0), P(t_0)) = (x_0, y_0, V_0, 0) \end{aligned} \quad (4)$$

where $\underline{u}_1 = \underline{K}$, $\underline{u}_2 = 1/\overline{R}$, $\overline{u}_1 = \overline{K}$ and $\overline{u}_2 = 1/\underline{R}$ are all positive constants.

3 Analysis of Optimal Controls

3.1 Pontryagin’s Maximum Principle

Let us start by introducing some terminology used in this work. A control $u: [t_0, t_f] \rightarrow [\underline{u}, \overline{u}]$ only switching between the lower and upper bounds of the compact control set, i.e., \underline{u} and \overline{u} , is called *bang–bang*, while it is called *singular*, if $u(t)$ takes values in the interior of the control set. We introduce $X(t) = (x(t), y(t), V(t), P(t))^T$, $u(t) = (u_1(t), u_2(t))^T$ and

$$\begin{aligned} f(X(t), t) &= \left(y(t), \frac{\Gamma^2 x(t)}{mC} - \frac{by(t)}{m} - \frac{\Gamma V(t)}{m} + F(t), \frac{\Gamma y(t)}{C}, 0 \right)^T, \\ g_1(X(t)) &= \left(0, -\frac{x(t)}{m}, 0, 0 \right)^T, \quad g_2(X(t)) = \left(0, 0, -\frac{V(t)}{C}, V(t)^2 \right)^T, \end{aligned}$$

then the system of ODEs in (4) becomes

$$\dot{X}(t) = f(X(t), t) + g_1(X(t))u_1(t) + g_2(X(t))u_2(t) := R_d(X(t), t, u(t)). \quad (5)$$

Let us first recall the first-order necessary conditions for optimality of controls $u_1(t)$, $u_2(t)$ given by the classical Pontryagin's maximum principle (PMP) [13, 14]. The PMP says that, if $u_1^*(t)$, $u_2^*(t)$ are optimal controls with the corresponding optimal trajectories $(x^*(t), y^*(t), V^*(t), P^*(t))_T$ on the interval $[t_0, t_f]$, there exist a constant $p_0 > 0$ and an absolutely continuous adjoint vector $p: [t_0, t_f] \rightarrow \mathbb{R}^4$ such that

- (P1) Nontriviality of the multipliers: $(p_0, p(t)) \neq 0$ for all $t \in [t_0, t_f]$,
 (P2) Adjoint equations: $p(t)$ is the solution of the following adjoint equations

$$\begin{aligned} \dot{p}_1(t) &= -p_2(t) \left(\frac{\Gamma^2}{Cm} - \frac{u_1^*(t)}{m} \right), \\ \dot{p}_2(t) &= -p_1(t) + p_2(t) \frac{b}{m} - p_3(t) \frac{\Gamma}{C}, \\ \dot{p}_3(t) &= p_2(t) \frac{\Gamma}{m} + p_3(t) \frac{u_2^*(t)}{C} - 2p_4(t)u_2^*(t)V^*(t), \\ \dot{p}_4(t) &= 0, \end{aligned} \quad (6)$$

together with the transversality condition $p(t_f) = (0, 0, 0, p_0)$.

- (P3) Maximum condition: the optimal controls $u_1^*(t)$, $u_2^*(t)$ maximize the *Hamiltonian* H

$$H(X(t), p(t), t, u(t)) = \langle p(t), f(X(t), t) + g_1(X(t))u_1(t) + g_2(X(t))u_2(t) \rangle$$

along $(p(t), x^*(t), y^*(t), V^*(t), P^*(t))$ over $[\underline{u}_1, \bar{u}_1]$ and $[\underline{u}_2, \bar{u}_2]$, respectively, in particular

$$\begin{aligned} &H(X(t)^*, p(t), t, u^*(t)) \\ &= \max_{u_1(t) \in U_1, u_2(t) \in U_2} \langle p(t), f(X(t)^*, t) + g_1(X(t)^*)u_1(t) + g_2(X(t)^*)u_2(t) \rangle \\ &\quad \forall t \in [t_0, t_f], \quad \text{where } U_1 = [\underline{u}_1, \bar{u}_1], \quad U_2 = [\underline{u}_2, \bar{u}_2]. \end{aligned}$$

3.2 Synthesis of Optimal Controls via Switching Functions

Let us rewrite the Hamiltonian as

$$H(X(t), p(t), t, u(t)) = \langle p(t), f(X(t), t) \rangle + \Phi_1(t)u_1(t) + \Phi_2(t)u_2(t),$$

where $\Phi_1(t) = \langle p(t), g_1(X(t)) \rangle$, $\Phi_2(t) = \langle p(t), g_2(X(t)) \rangle$. The structures of the optimal controls are determined by the properties of the switching functions

$\Phi_1(t), \Phi_2(t)$. As long as $\Phi_1(t), \Phi_2(t)$ are not zero, due to the maximum condition (P3) of PMP, the optimal controls are given by

$$u_1^*(t) = \begin{cases} \underline{u}_1, & \text{if } \Phi_1(t) < 0, \\ \overline{u}_1, & \text{if } \Phi_1(t) > 0, \end{cases} \quad u_2^*(t) = \begin{cases} \underline{u}_2, & \text{if } \Phi_2(t) < 0, \\ \overline{u}_2, & \text{if } \Phi_2(t) > 0. \end{cases} \tag{7}$$

The optimal controls cannot be determined directly by the maximum condition if $\Phi_1(t), \Phi_2(t)$ are equal to zero on a sub-interval with positive measure. In this case, some information about the structures of optimal controls can be obtained by analyzing the time derivatives of the switching functions, see, e.g., [13, Chapter 2].

In general, the optimal controls are synthesized from potential candidates of optimality which are concatenations of bang–bang and singular arcs via the analysis of the zero sets of $\Phi_1(t), \Phi_2(t)$

$$Z_1 = \{t \in [t_0, t_f] : \Phi_1(t) = 0\}, \\ Z_2 = \{t \in [t_0, t_f] : \Phi_2(t) = 0\}.$$

3.3 Analysis of Optimal Controls

Observe that the vector $(p_0, p(t))$ can be normalized since $p_0 > 0$. Therefore, without loss of generality, we assume that $p_0 = 1$ which leads to $p_4(t) = 1$ for all $t \in [t_0, t_f]$. In the following, we will prove that Z_1, Z_2 are countable, i.e., $\Phi_1(t), \Phi_2(t)$ have countable switchings. Consequently the potential candidates of the optimal controls $u_1(t), u_2(t)$ for the problem (4) are of bang–bang type. We have

$$\Phi_1(t) = \langle p(t), g_1(X(t)) \rangle = -p_2(t) \frac{x(t)}{m}, \\ \Phi_2(t) = \langle p(t), g_2(X(t)) \rangle = -p_3(t) \frac{V(t)}{C} + p_4(t)V(t)^2 = -p_3(t) \frac{V(t)}{C} + V(t)^2.$$

It is easy to obtain the first derivatives of $\Phi_1(t)$ and $\Phi_2(t)$ as

$$\dot{\Phi}_1(t) = p_1(t) \frac{x(t)}{m} - p_2(t) \left(\frac{bx(t)}{m^2} + \frac{y(t)}{m} \right) + p_3(t) \frac{\Gamma x(t)}{Cm}, \\ \dot{\Phi}_2(t) = -p_2(t) \frac{\Gamma V(t)}{Cm} - p_3(t) \frac{\Gamma y(t)}{C^2} + \frac{2\Gamma V(t)y(t)}{C}.$$

Obviously, if $\Phi_1(t) = 0$ and $\dot{\Phi}_1(t) \neq 0$ ($\Phi_2(t) = 0$ and $\dot{\Phi}_2(t) \neq 0$), $u_1(t)$ ($u_2(t)$) switches between \underline{u}_1 and \overline{u}_1 (\underline{u}_2 and \overline{u}_2). We are going to show that there exists no time interval on which both $\Phi_1(t)$ and all its derivatives of $\Phi_1(t)$ vanish, i.e., $u_1(t)$ is a bang–bang control. Similarly, we will point out that $u_2(t)$ is also a bang–bang control.

Remark 3.1 There exists no time interval $(t_1, t_2) \subset [t_0, t_f]$ on which $V(t) \equiv 0, \forall t \in (t_1, t_2)$ since otherwise the system of ODEs in (4) has no solution for any controls $u_1(t), u_2(t)$ and either of the nonzero external forces in $F(t)$ (3).

Proposition 3.1 *The switching function $\Phi_1(\cdot)$ has a countable number of switchings over $[t_0, t_f]$ and therefore the optimal control $u_1(t)$ is of a bang–bang type.*

Proof We are going to prove this proposition by assuming contradictorily that there exists $(t_1, t_2) \subset [t_0, t_f]$ on which $\Phi_1(t)$ and all its derivatives vanish. We have

$$\Phi_1(t) = -p_2(t) \frac{x(t)}{m} = 0,$$

which leads to either $p_2(t) = 0$ or $x(t) = 0$.

(i) if $p_2(t) = 0$, then owing to (6) we have

$$\begin{aligned} \dot{p}_1(t) &= 0, \\ \dot{p}_2(t) &= -p_1(t) - p_3(t) \frac{\Gamma}{C}, \\ \dot{p}_3(t) &= p_3(t) \frac{u_2(t)}{C} - 2u_2(t)V(t), \\ p_4(t) &= 1. \end{aligned}$$

Since $p_2(t) = 0$ on (t_1, t_2) , $\dot{p}_2(t) = 0$. Thus from the above system we derive $p_1(t) = -p_3(t) \frac{\Gamma}{C}$, therefore $\dot{\Phi}_1(t) = 0$.

By differentiating both sides of $p_1(t) = -p_3(t) \frac{\Gamma}{C}$ and taking into account $\dot{p}_1(t) = 0$, we obtain $\dot{p}_1(t) = -\dot{p}_3(t) \frac{\Gamma}{C}$ which implies $\dot{p}_3(t) = 0$ and $p_3(t) = 2CV(t)$ for $u_2(t) \neq 0$. Therefore, $\dot{V}(t) = 0$ which means $V(t) = V(t_1) = V_c$, where V_c is a nonzero constant due to Remark 3.1 and V_c does not depend on $u_2(t)$ with $t \in (t_1, t_2)$. Since $\dot{P}(t) = V(t)^2 u_2(t) = V_c^2 u_2(t)$ over (t_1, t_2) , see (4), in order to gain the maximum power $u_2(t)$ has to be chosen as the upper bound, i.e., $u_2(t) = \bar{u}_2$. This violates (7) since according to (7)

$$\Phi_2(t) = \langle p(t), g_2(X(t)) \rangle = -V^2(t) = -V_c^2 < 0$$

implies $u_2(t) = \underline{u}_2$. Therefore, there is no time interval on which $\Phi_1(t)$ and all its derivatives vanish, i.e., $u_1(t)$ switches between $\underline{u}_1, \bar{u}_1$, or in other words $u_1(t)$ is a bang–bang control.

(ii) if $x(t) = 0$, $p_2(t) \neq 0$, due to (4) we obtain also $y(t) = 0$ and

$$V(t) = \frac{m}{F} F(t), \quad \dot{V}(t) = \frac{-u_2(t)}{C} V(t),$$

which implies

$$u_2(t) = \frac{-\dot{F}(t)C}{F(t)} \tag{8}$$

when $\{t : F(t) = 0\} \cap (t_1, t_2) = \emptyset$ [since $F(t)$ in (3) has finite zeros on $[t_0, t_f]$, it

is always possible to take (t_1, t_2) such that the intersection is an empty set]. On the other hand, if $\Phi_2(t) \neq 0$, we conclude immediately that u_2 is a bang–bang control due to (7). Otherwise we have $\dot{\Phi}_2(t) = -p_2(t) \frac{\Gamma V(t)}{Cm} \neq 0$ on (t_1, t_2) due to Remark 3.1 which implies that $u_2(t)$ switches finitely between \underline{u}_2 and \overline{u}_2 . Both cases result in a contradiction to (8).

Therefore $\Phi_1(t)$ and its derivatives cannot vanish on any time interval $(t_1, t_2) \subset [t_0, t_f]$ which means that $u_1(t)$ is only of a bang–bang type. \square

Remark 3.2 From a physical point of view, in Case (i) in the proof of Proposition 3.1, if $\dot{V}(t) = 0$ on some interval (t_1, t_2) , in principle $\overline{u}_2 = \frac{1}{R}$ can be chosen large enough to maximize the output power. Then

$$P = \frac{1}{t_2 - t_0} \left(\int_{t_0}^{t_1} V(s)^2 u_2(s) ds + (t_2 - t_1) \frac{V_c^2}{R} \right) \xrightarrow{R \rightarrow 0} +\infty$$

which is unphysical, i.e., $\dot{V}(t) \neq 0$.

Similarly, we derive the following proposition which determines the structure of $u_2(t)$.

Proposition 3.2 *The switching function $\Phi_2(\cdot)$ has a countable number of switchings over $[t_0, t_f]$, i.e., the optimal control candidate $u_2(t)$ is of a bang–bang type.*

Proof Assume there exists $(t_1, t_2) \subset [t_0, t_f]$ such that $\Phi_2(t)$ and all derivatives vanish for every t in (t_1, t_2) . Owing to $\Phi_2(t) = 0$ and $\dot{\Phi}_2(t) = 0$ we have

$$p_3(t) = CV(t), \quad p_2(t) = y(t)m. \tag{9}$$

By substituting (9) into the adjoint equations in (6), we receive

$$\begin{aligned} \dot{p}_1(t) &= -y(t) \left(\frac{\Gamma^2}{C} - u_1(t) \right), & p_1(t_f) &= 0, \\ \dot{p}_2(t) &= -p_1(t) + y(t)b - V(t)\Gamma, & p_2(t_f) &= 0, \\ \dot{p}_3(t) &= y(t)\Gamma - V(t)u_2(t), & p_3(t_f) &= 0, \\ p_4(t) &= 1, & p_4(t_f) &= 1. \end{aligned} \tag{10}$$

Observe after taking the derivative on both sides of $p_2(t) = y(t)m$ and using (10) in connection with the dynamics in (4), we have, for $t \in (t_1, t_2)$,

$$\begin{aligned} p_1(t) &= 2by(t) + \left(u_1(t) - \frac{\Gamma^2}{C} \right) x(t) - mF(t), \\ \dot{p}_1(t) &= -y(t) \left(\frac{\Gamma^2}{C} - u_1(t) \right) \end{aligned} \tag{11}$$

which has a solution if and only if $\dot{y}(t) = \frac{m}{2b}\dot{F}(t)$ since $u_1(t)$ is a bang–bang control, see Proposition 3.1. Owing to $\dot{y}(t) = \frac{m}{2b}\dot{F}(t)$ and (4), we obtain

$$\frac{m}{2b}\dot{F}(t) = -\frac{1}{m}\left(u_1(t) - \frac{\Gamma^2}{C}\right)x(t) - \frac{b}{m}y(t) - \frac{V(t)\Gamma}{m} + F(t) \quad (12)$$

or reordered

$$V(t) = \frac{-\left(u_1(t) - \frac{\Gamma^2}{C}\right)x(t) - by(t) + mF(t) - \frac{m^2}{2b}\dot{F}(t)}{\Gamma}.$$

By making use of $\dot{V}(t) = \frac{\Gamma y(t)}{C} - \frac{u_2(t)}{C}V(t)$ and $\dot{u}_1(t) = 0$ due to Proposition 3.1, we have

$$u_2(t) = \frac{Cu_1(t)y(t) - \frac{Cm}{2}(\dot{F}(t) - \frac{m}{b}\ddot{F}(t))}{-\left(u_1(t) - \frac{\Gamma^2}{C}\right)x(t) - by(t) + mF(t) - \frac{m^2}{2b}\dot{F}(t)}. \quad (13)$$

Let V_c, y_c, x_c be some constants such that the solution of

$$\begin{aligned} \dot{V}(t) &= \frac{\Gamma y(t)}{C} - \frac{u_2(t)}{C}V(t), \\ \dot{y}(t) &= \frac{m}{2b}\dot{F}(t), \quad \dot{x}(t) = y(t) \end{aligned}$$

on $t \in [t_1, t_2]$ reads as follows

$$\begin{aligned} V(t) &= e^{-\int_{t_1}^t \frac{u_2(s)}{C} ds} V_c + \frac{\Gamma}{C} \int_{t_1}^t e^{-\int_s^t \frac{u_2(w)}{C} dw} y(s) ds, \\ y(t) &= y_c + \frac{m}{2b}F(t), \\ x(t) &= x_c + y_c t + \frac{m}{2b} \int_{t_1}^t F(s) ds. \end{aligned} \quad (14)$$

Moreover, observe that (12) is equivalent to

$$u_1(t) = \frac{-by(t) - \Gamma V(t) + mF(t) - \frac{m^2}{2b}\dot{F}(t)}{x(t)} + \frac{\Gamma^2}{C}. \quad (15)$$

By subsequently plugging (13), (14) and (3) into (15), $u_1(t)$ becomes a function of $u_1(t)$ whose solution, i.e., $u_1(t)$, cannot be a constant. This means that $u_1(t)$ has to be a singular control which is a contradiction to Proposition 3.1. Therefore, $u_2(t)$ switches between $\underline{u}_2, \bar{u}_2$ on (t_1, t_2) . In conclusion, $u_2(t)$ is always a bang–bang control. \square

Taking into account two of the preceding propositions, we obtain the following result.

Corollary 3.1 Consider the optimization problem (4), the optimal controls $u_1(t)$, $u_2(t)$ are bang–bang.

Proof It is a combination of Propositions 3.1 and 3.2.

4 Numerical Optimization and Discussion

In this section, we present numerical solutions of different optimal control problems and compare them with reference solutions from LT-SPICE simulations. The control problems are numerically challenging due to the highly stiff ODE system and different ranges of parameter values that are involved. As a heuristic, we calculate a suboptimal solution by aggregating N solutions on smaller time horizons $[t_i, t_{i+1}]$, $i = 0, \dots, N - 1$, instead of solving the optimization problem at once on the whole time interval $[t_0, t_f]$. We solve the problem (4) on each sub-interval $[t_i, t_{i+1}]$ with the initial state $X(t_i)$ taken from the terminal state solution $X(t_i)$ of the preceding sub-interval $[t_{i-1}, t_i]$, and $X(t_0) = (0, 0, 0, 0)$, $t_0 = 0$. The numerical results of the problem (4) on $[t_i, t_{i+1}]$ are obtained with the help of the open-source software tool CasADi [22] with Python interface. The ODE system is discretized and solved by CVODES from the SUNDIALS integrator suite, see [23] and the obtained nonlinear optimization problem is solved with IPOPT [24].

Observe that the system of ODEs in (4) is highly stiff due to the high drive frequency and needs to be approximated by suitable numerical methods with a sufficiently small time step size. For this particular problem, the time step is chosen to be smaller than 10^{-5} for the stability of the numerical solutions. The controls $u_1(t)$ and $u_2(t)$ are discretized with a step size of 2×10^{-5} .

The aggregated trajectory $X(\cdot)$ on $[t_0, t_f]$ is not necessarily optimal, but provides an estimate for the possible improvement compared to state-of-the-art operation. Simulations with fixed controls $K(t) = K_1$ and $R(t) = R_L$ can be carried out in LT-SPICE simulator and are used as reference solutions. The device parameters are adapted from [25] and listed in Table 1. Parameters of the linear two-port model are then [26]

Table 1 Example parameters for comb-drive capacitive transducers

| Parameters | Value |
|--------------------------------|---------------------------|
| Proof mass, m | 1.5 mg |
| Linear spring stiffness, k_m | 3 N m ⁻¹ |
| Thin-film air damping, b | 2.4e-5 Ns m ⁻¹ |
| Nominal capacitance, C_0 | 0.47 pF |
| Parasitic capacitance, C_p | 7.5 pF |
| Load capacitance, C_L | 8.6 pF |
| Nominal overlap, x_0 | 10 μm |
| Load resistance, R_L | 16.9 MΩ |
| Bias voltage, V_b | 24.9 V |

$$C = \frac{C_0 + C_p + C_L}{2}, \quad \Gamma = \frac{C_0 V_b}{x_0}, \quad K_1 = k_m + \frac{2C_0^2 V_b^2}{x_0^2 (C_0 + C_p + C_L)}.$$

The load resistance R_L and the open-circuit stiffness K_1 used in the lumped-model are kept fixed at the optimal value of the linear regime, adapted from [8], while the mechanical stiffness is a constant achieved from design. We will now consider the optimal problem in two cases: (i) no restrictions on proof mass motion and (ii) a constraint for displacement is taken into account.

4.1 Power Optimization for Unconstrained Displacement

Here, we consider the optimal performance of a harvester represented by a mass–spring–damping system without any limit on mass motion. The displacement $x(t)$ therefore only depends on the external excitation level, drive frequency and damping constants [27].

4.1.1 Acceleration Sweep

A sinusoidal acceleration sweep vibration input $F(t) = F_a(t) = A_f t g \cos(\omega t)$ is examined, where $t \in [t_0, t_f] = [0, 1]$ s, $A_0 = 0$ g and $A_f = 0.05$ g leading to $A_f = 0.05$ g s⁻¹. The drive frequency is chosen as $\omega = \sqrt{\frac{K_1}{m}}$. Figure 3 shows the parameterized stiffness $\delta k = (K(t) - m\omega^2)/\omega b$ and the electrical time constant $\omega\tau = \omega R(t)C$, with $K(t) = u_1(t)$ and $R(t) = 1/u_2(t)$, after optimization. The *bang–bang* behavior of both physically important variables δk and $\omega\tau$ is identical to the theoretical analysis in Sect. 3, with $\delta k \in [0, 10]$ and $\omega\tau \in [\frac{1}{100}, 1]$, except for some control values due to numerical errors.

Figure 4 presents the harvested power achieved with optimized controls compared to the reference solution with fixed controls from LT-SPICE. The optimized control strategy improves the harvested power outcome by 227%. The bang–bang characteristic of the optimal controls is still true for the following case.

4.1.2 Frequency Sweep

In this case study, instead of varying the acceleration amplitude, a linear swept-frequency cosine signal at the time instances $t \in [t_0, t_f] = [0, 2]$ s is investigated, where $F(t) = F_f(t) = A_c g \cos(\omega_0 t + \frac{1}{2}\omega_f t^2)$ with $A_c = 0.05$ g, $\omega_0 = 200\pi$ rad s⁻¹ and $\omega_f = 800\pi$ rad s⁻¹. Thus, the swept rate of angular frequency is $\omega_f = 300\pi$ rads⁻². The numerical optimization of the output power is depicted in Fig. 5 with more than five times higher than that of the results obtained from LT-SPICE.

4.2 Power Optimization under Displacement-Constraint Operation

In practical energy harvesters, the proof mass displacement must be restricted to avoid spring fracture under high input acceleration amplitudes, or to be confined in the finite

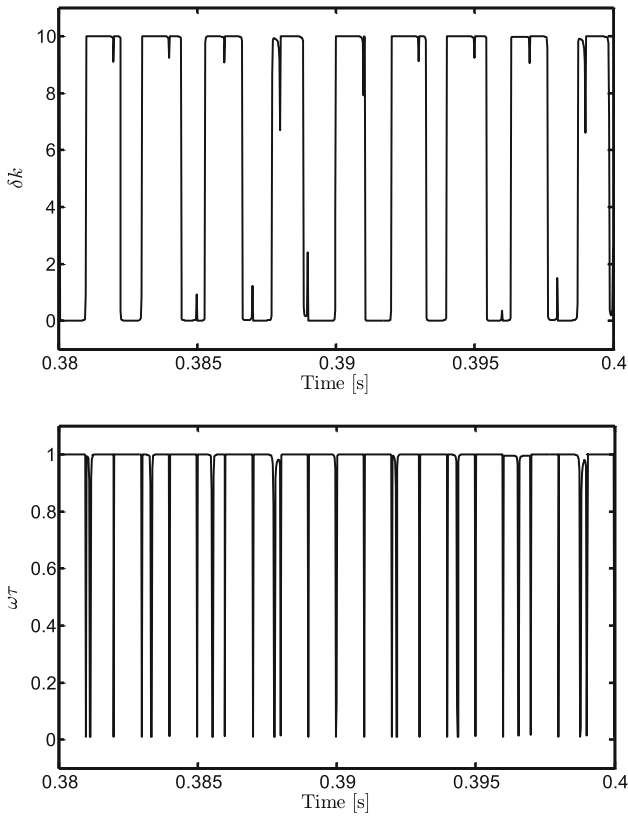


Fig. 3 Closed-view waveforms of the parameterized stiffness $\delta k = (K(t) - m\omega^2)/\omega b$ and the parameterized load $\omega\tau = \omega R(t)C$

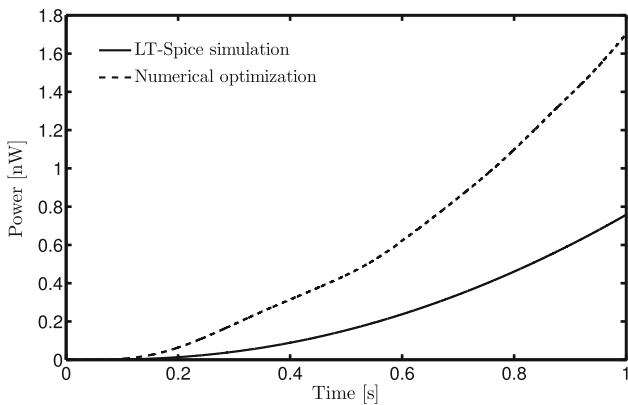


Fig. 4 Numerical optimization result in comparison with simulation obtained from LT-SPICE for the amplitude sweep of external acceleration

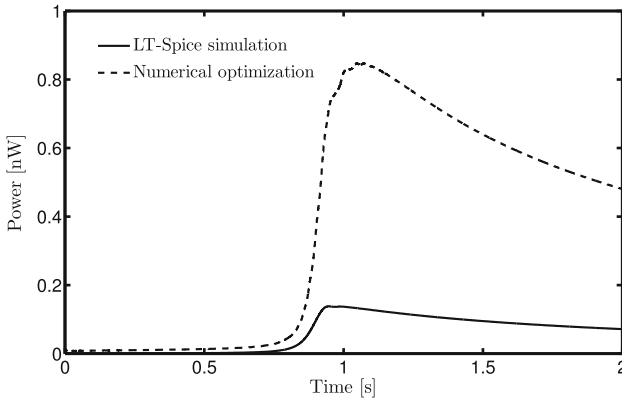


Fig. 5 Numerical optimization result in comparison with simulation for the frequency-sweep excitation

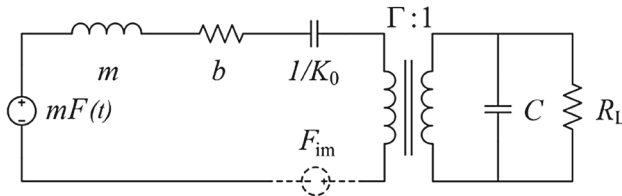


Fig. 6 Two-port model in LT-SPICE with impact force between the proof mass and the end-stops

dimensions of real structures. This can be implemented by designing mechanical end-stops. In the LT-SPICE simulation, the impact mechanism during the contact period is modeled as Hertzian contact force, as shown in Fig. 6. The impact force may then be written as a function of the relative displacement between the proof mass and the rigid end-stops $\delta = |x(t)| - X_{\max}$ for $|x(t)| \geq X_{\max}$, see [28]

$$F_{\text{im}} = k_{\text{im}} \delta^{\frac{3}{2}} \left(1 + \frac{3}{4} \frac{\dot{\delta}}{\delta_-} (1 - e^2) \right) \tag{16}$$

where $X_{\max} = 5.5 \mu\text{m}$, $k_{\text{im}} = 3.361 \text{ MN}$, m^{-1} is the impact stiffness, $\delta_- = 8 \text{ mm s}^{-1}$ is the impact velocity and $e = 0.7$ is the coefficient of restitution. See [25] for a detailed analysis. Due to the special characteristics of the impact force [29,30], the numerical optimization problem (2), in which the second-order ODE is replaced by $m\ddot{x}(t) = -\left(K(t) - \frac{\Gamma^2}{C}\right)x(t) - b\dot{x}(t) - V(t)\Gamma + mF(t) - F_{\text{im}}$, is too challenging. Therefore, in this case, we consider the problem (2) affiliated with the condition $\frac{|x(t)|}{X_{\max}} \leq 1$ instead. Other parameters for acceleration sweep and frequency sweep forces are the same as in Sect. 4.1.

Notice that the behavior of optimal controls under displacement-constrained operation has not been theoretically investigated in this work, while numerical optimizations are provided as additional case studies.

4.2.1 Acceleration Sweep

Figure 7 illustrates the numerical solution of optimal extracted power which is about 2.5 times higher compared to the result achieved from simulation.

4.2.2 Frequency Sweep

The optimal value of the harvested power is solved numerically and presented in Fig. 8. However, the improvement of output power is not much when t is in the range of $[1.25, 2]$ s. This can be explained by the difference between the behavior of the impact force in the lumped-model simulation and the mathematical condition $|x(t)| \leq X_{\max}$ used for problem (2). Micro-electro-mechanical systems (MEMS) energy harvesters exploiting impacts through alternative configurations were reported in [31–34], with both modeling and experimental validations. These works exhibit the bandwidth enhancement in up-frequency sweep, i.e., going from low toward high frequencies. This phenomenon cannot be performed without a Hertzian contact model or piecewise-linear restoring force, as in problem (2). Figure 9 shows the comparison of proof mass displacement as evidence for the mentioned assertion.

In summary, this work indicated the optimal behavior of the two control subjects, load and stiffness, in order to maximize the extracted power of the vibration energy harvesters under unconstrained displacement. The numerical optimization results show significant enhancements in transducer performances with different input forces and operating conditions. This is clearly an encouragement for future research on optimization on the whole time horizon. Owing to the bang–bang property, the resistive load and open-circuit stiffness now only need to be switched between upper and lower bounds which is of convenience for designing in practice, instead of being adjusted to achieve each optimal value when the input driving force changes as analysis of previous works from other authors has shown. It is worth noting that the optimal output power here is only a local value depending on the setting of parameterized stiffness

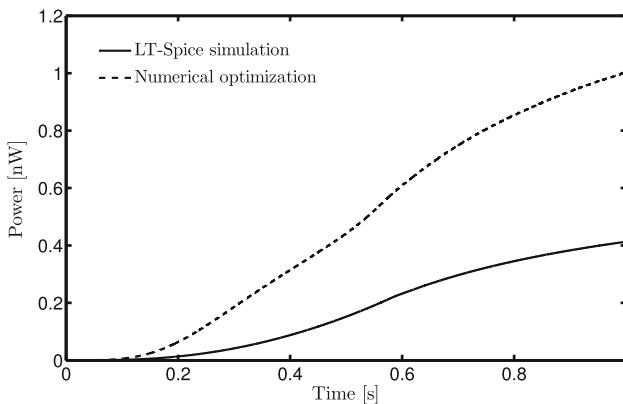


Fig. 7 Numerical optimization results in comparison with simulation for the amplitude sweep of external acceleration, under displacement-constrained operation

and electrical time constant bounds, see Fig. 10 for instance. The magnitude of these ranges can be appropriately chosen so that the global optimal value is achieved. An analysis of the optimal behavior of the load and stiffness along with limitation of the mathematical model under displacement-constrained operation is also a promising problem which needs to be addressed.

Last but not least, there is work done in changing the time-varying stiffness at fixed displacement, which is given by $P_K = \frac{1}{2}x^2dK$. Considering the net power harvested by the transducers, one would expect to reformulate the integrand of the objective function in (2), i.e., instead of $\frac{V^2}{R}$ it should be $(\frac{V^2}{R} - P_K)$. This is an open issue for further investigations.

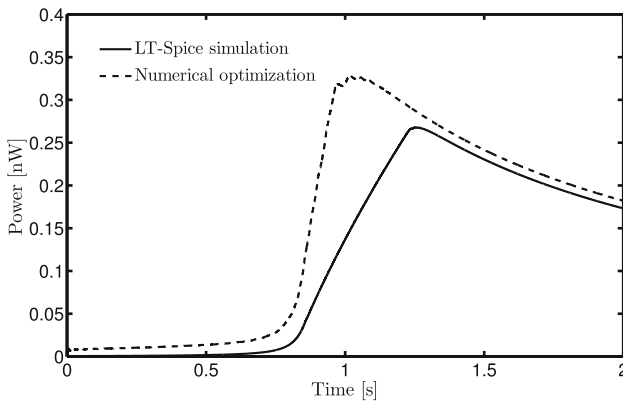


Fig. 8 Numerical optimization and simulation results for the frequency-sweep excitation, with restriction of displacement

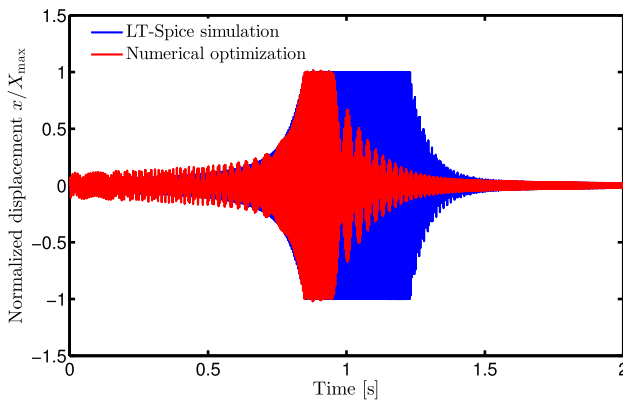


Fig. 9 Comparison of the proof mass displacement in two cases: (i) numerical optimization and (ii) simulation, for the frequency-sweep sinusoidal input

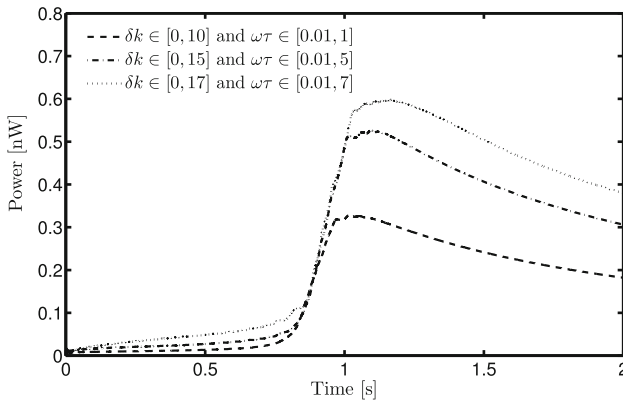


Fig. 10 Comparison of the optimal output power with different ranges of the parameterized stiffness and the electrical time constant

5 Conclusions

This work investigated the optimal behavior of the load and stiffness to maximize the extracted power of vibration energy harvesters under unconstrained displacement operation. Significant enhancements in transducer performances are observed from the numerical optimization results. In order to obtain the optimal output power, due to the bang–bang property, the resistive load and open-circuit stiffness are switched only between their upper and lower bounds, which is of convenience for designing the harvesting system in practice.

Acknowledgements Financial support from the European Research Council via the Consolidator Grant MODEST-647573 is gratefully acknowledged. Thanks to Prof. Giovanni Colombo for his valuable suggestions and to Robert Rantz for proofreading the article.

References

1. Mitcheson, P.D., Yeatman, E.M., Rao, G.K., Holmes, A.S., Green, T.C.: Energy harvesting from human and machine motion for wireless electronic devices. *Proc. IEEE* **96**(9), 1457–1486 (2008)
2. Roundy, S., Wright, P.K., Rabaey, J.: A study of low level vibrations as a power source for wireless sensor nodes. *Comput. Commun.* **26**(11), 1131–1144 (2003)
3. Ottman, G., Hofmann, H., Bhatt, A., Lesieutre, G.: Adaptive piezoelectric energy harvesting circuit for wireless remote power supply. *IEEE Trans. Power Electron.* **17**(5), 669–676 (2002)
4. Renno, J.M., Daqaq, M.F., Inman, D.J.: On the optimal energy harvesting from a vibration source. *J. Sound Vib.* **320**, 386–405 (2008)
5. Mitcheson, P.D., Green, T.C., Yeatman, E.M., Holmes, A.S.: Architectures for vibration-driven micropower generators. *J. Microelectromech. Syst.* **13**(3), 429–440 (2004)
6. Halvorsen, E., Le, C.P., Mitcheson, P.D., Yeatman, E.M.: Architecture-independent power bound for vibration energy harvesters. *J. Phys. Conf. Ser.* **476**(1), 012–026 (2013)
7. Heit, J., Roundy, S.: A framework to determine the upper bound on extractable power as a function of input vibration parameters. *Energy Harvest. Syst.* **3**(1), 069–078 (2015)
8. Halvorsen, E.: Optimal load and stiffness for displacement-constrained vibration energy harvesters. *ArXiv e-prints* (2016)

9. Marboutin, C., Suzuki, Y., Kasagi, N.: Vibration-driven MEMS energy harvester with vertical electrets. In: *Proceedings of the PowerMEMS*, pp. 141–144. Freiburg, Germany (2007)
10. Erturk, A., Inman, D.J.: Parameter identification and optimization in piezoelectric energy harvesting: analytical relations, asymptotic analyses, and experimental validations. *Proc. Inst. Mech. Eng. I J. Syst. Control Eng.* **225**(4), 485–496 (2011)
11. Le, C.P., Halvorsen, E., Søråsen, O., Yeatman, E.M.: Microscale electrostatic energy harvester using internal impacts. *J. Intell. Mater. Syst. Struct.* **23**, 1409–1421 (2012)
12. von Büren, T., Tröster, G.: Design and optimization of a linear vibration-driven electromagnetic micro-power generator. *Sens. Actuators A* **135**(2), 765–775 (2007)
13. Schättler, H., Ledzewicz, U.: *Geometric Optimal Control: Theory, Methods and Examples*, vol. 38. Springer, Berlin (2012)
14. Bressan, A., Piccoli, B.: *Introduction to the Mathematical Theory of Control*, vol. 2. American Institute of Mathematical Sciences, Springfield (2007)
15. Ledzewicz, U., Schättler, H.: Antiangiogenic therapy in cancer treatment as an optimal control problem. *SIAM J. Control Optim.* **46**(3), 1052–1079 (2007)
16. d’Onofrio, A., Ledzewicz, U., Maurer, H., Schättler, H.: On optimal delivery of combination therapy for tumors. *Math. Biosci.* **222**(1), 13–26 (2009)
17. Ledzewicz, U., Mosalman, M.S.F., Schättler, H.: Optimal controls for a mathematical model of tumor-immune interactions under targeted chemotherapy with immune boost. *Discrete Contin. Dyn. Syst. Ser. B* **18**(4), 1031–1051 (2013)
18. Sager, S.: Sampling decisions in optimum experimental design in the light of Pontryagin’s maximum principle. *SIAM J. Control Optim.* **51**(4), 3181–3207 (2013)
19. Grigorieva, E., Khailov, E.: Optimal control of a nonlinear model of economic growth. In: *Discrete and Continuous Dynamical Systems*, pp. 456–466 (2007)
20. Grigorieva, E.V., Khailov, E.N.: Hierarchical differential game between manufacturer, retailer, and bank. *J. Dyn. Control Syst.* **15**(3), 359–391 (2009)
21. Tilmans, H.A.C.: Equivalent circuit representation of electromechanical transducers: I. Lumped-parameter systems. *J. Micromech. Microeng.* **6**, 157–176 (1996)
22. Andersson, J., Åkesson, J., Diehl, M.: CasADI: a symbolic package for automatic differentiation and optimal control. In: Barth, T.J., Griebel, M., Keyes, D.E., Nieminen, R.M., Roose, D., Schlick, T. (eds.) *Recent Advances in Algorithmic Differentiation*, pp. 297–307. Springer, Berlin (2012)
23. Hindmarsh, A.C., Brown, P.N., Grant, K.E., Lee, S.L., Serban, R., Shumaker, D.E., Woodward, C.S.: SUNDIALS: suite of nonlinear and differential/algebraic equation solvers. *ACM Trans. Math. Softw. (TOMS)* **31**(3), 363–396 (2005)
24. Wächter, A., Biegler, L.T.: On the implementation of an interior-point filter line-search algorithm for large-scale nonlinear programming. *Math. Program.* **106**(1), 25–57 (2006)
25. Truong, B.D., Le, C.P., Halvorsen, E.: Power optimization and effective stiffness for a vibration energy harvester with displacement constraints. *J. Micromech. Microeng.* **26**(12), 124,006 (2016)
26. Le, C.P., Halvorsen, E.: MEMS electrostatic energy harvesters with end-stop effects. *J. Micromech. Microeng.* **22**(7), 74013–74024 (2012)
27. Williams, C.B., Yates, R.B.: Analysis of a micro-electric generator for microsystems. *Sens. Actuators A* **52**(1–3), 8–11 (1996)
28. Lankarani, H.M., Nikravesh, P.E.: Continuous contact force models for impact analysis in multibody systems. *Nonlinear Dyn.* **5**(2), 193–207 (1994)
29. Babitsky, V., Krupenin, V.: *Vibration of Strongly Nonlinear Discontinuous Systems Engineering Online Library*. Springer, Berlin (2001)
30. Manevitch, L.I., Gendelman, O.V.: Oscillatory models of vibro-impact type for essentially non-linear systems. *Proc. Inst. Mech. Eng. C J. Mech. Eng. Sci.* **222**(10), 2007–2043 (2008)
31. Soliman, M., Abdel-Rahman, E., El-Saadany, E., Mansour, R.: A design procedure for wideband micropower generators. *J. Microelectromech. Syst.* **18**(6), 1288–1299 (2009)
32. Hoffmann, D., Folkmer, B., Manoli, Y.: Fabrication, characterization and modelling of electrostatic micro-generators. *J. Micromech. Microeng.* **19**(9), 094001 (2009)
33. Liu, H., Tay, C.J., Quan, C., Kobayashi, T., Lee, C.: Piezoelectric MEMS energy harvester for low-frequency vibrations with wideband operation range and steadily increased output power. *J. Microelectromech. Syst.* **20**(5), 1131–1142 (2011)
34. Le, C.P., Halvorsen, E.: An electrostatic energy harvester with end-stop effects. In: *Proceedings of the 22nd Micromechanics and Microsystem Technology Europe Workshop*. Tønsberg, Norway (2011)